Nanoscale Advances

ROYAL SOCIETY OF CHEMISTRY

PAPER

View Article Online
View Journal | View Issue

Cite this: *Nanoscale Adv.*, 2024, **6**, 6408

Synthesis of a novel nanomagnetic N_4 bis schiff base complex of copper(II) as an efficient catalyst for click synthesis of tetrazoles

Chou-Yi Hsu,[a] Ahmed Rafiq AlBajalan,[*b] Sameer A. Awad,[c] Muath Suliman,[d] Nizomiddin Juraev,[ef] Carlos Rodriguez-Benites,[g] Hamad AlMohamadi[h] and Abed J. Kadhim[i]

Received 1st August 2024
Accepted 22nd October 2024

DOI: 10.1039/d4na00642a

rsc.li/nanoscale-advances

In this study, we have prepared a novel bis-Schiff-base copper(II) complex by modifying Fe_3O_4 with acetylacetone functionalities and subsequently forming a Schiff base with 2-picolylamine and $CuCl_2$ through a template method. Immobilization of 2,4-pentanedione and its reaction with 2-picolylamine enabled the synthesis of 1,3-diketimines (HNacNac) as an anionic ligand. This unique design resulted in a tetradentate N_4 coordination sphere for copper(II) ion complexation. The resulting heterogeneous catalyst, [Fe_3O_4@Sil-Schiff-base-Cu(II)], efficiently catalyzed the click condensation of diverse aryl nitriles with sodium azide to produce 5-substituted 1*H*-tetrazoles in high yields and selectivity. The catalyst demonstrated remarkable stability and recyclability without appreciable loss of catalytic activity, as confirmed by hot filtration and reusability studies.

1. Introduction

Tetrazoles are indispensable nitrogen rich aromatic heterocyclic scaffolds that offer a broad spectrum of applications in various domains such as medicinal chemistry, high energy material science, biochemistry, pharmacology *etc.* They do not exist in nature and their preparation often involves artificial methods.[1,2] Tetrazoles can be synthesized through various methods, including the Schmidt reaction, 1,3-dipolar cycloaddition, and click chemistry. Catalysts like copper(I) salts, gold(I) complexes, and organic catalysts play a crucial role in enhancing reaction efficiency and selectivity.[3–8] In this sense, click chemistry is indeed a particularly valuable approach in tetrazole synthesis.[9–11] Its high efficiency, selectivity, and mild reaction conditions make it an ideal tool for constructing complex tetrazole-containing molecules.[12] The transition metals catalyzed azide–alkyne cycloaddition is the most prominent click reaction in this context.[13,14] By employing this strategy, researchers can rapidly build diverse tetrazole libraries for drug discovery, materials science, and other applications.[15]

Creating organic compounds through chemical reactions while protecting the environment is a major challenge in organic chemistry.[16] The increasing concern for the planet has made it essential to find eco-friendly ways to perform these reactions. Therefore, scientists are actively searching for new catalysts that can produce desired compounds without harming the environment.[17] Recent advancements have seen heterogeneous materials emerge as efficient catalysts for tetrazole synthesis, offering advantages like high surface area and ease of modification.[8,18] These developments have expanded the possibilities for creating diverse tetrazole derivatives with potential applications in medicine, agriculture, and materials science.[19–21] These studies have investigated a variety of materials as foundations for catalysts, such as graphene oxide,[22] MCM-41,[23] SBA-15, charcoal,[24] boehmite[13] and magnetic nanoparticles.[25,26] Among these, magnetic nanoparticles composed of magnetite have garnered significant attention. Their magnetic properties enable rapid and convenient separation, while their biocompatibility, cost-effectiveness, and durability make them ideal for industrial processes.[27,28] As a result, these nanoparticles have been employed across numerous applications, including catalysis and biomedical technologies.[29]

[a]*Thunderbird School of Global Management, Arizona State University Tempe Campus, Phoenix, Arizona 85004, USA*

[b]*Petroleum Technology Department, Erbil Polytechnic University, Erbil, Kurdistan Region, Iraq. E-mail: ahmedrafiqalbajalan@gmail.com; ahmed.al_bajalan@epu.edu.iq*

[c]*Department of Medical Laboratories Techniques, College of Health and Medical Technology, University of Al Maarif, Al Anbar, 31001, Iraq*

[d]*Department of Clinical Laboratory Sciences, College of Applied Medical Sciences, King Khalid University, Abha, Saudi Arabia*

[e]*Researcher, Faculty of Chemical Engineering, New Uzbekistan University, Tashkent, Uzbekistan*

[f]*Scientific and Innovation Department, Tashkent State Pedagogical University, Tashkent, Uzbekistan*

[g]*Universidad Nacional de Trujillo, Trujillo, Peru*

[h]*Department of Chemical Engineering, Faculty of Engineering, Islamic University of Madinah, Madinah, Saudi Arabia*

[i]*Department of Medical Engineering, Al-Nisour University College, Baghdad, Iraq*

A variety of metal-based catalyst complexes have been immobilized on magnetic supports for diverse applications.[30–32] Among these, copper complexes derived from Schiff bases have attracted considerable attention due to their facile synthesis and potential catalytic activity.[33,34] Conventional approaches for immobilizing Schiff base ligands on magnetic nanoparticles typically involve the nucleophilic reaction of amine-functionalized supports with aldehydes or ketones.[34–36] However, the heterogeneous distribution of amine groups on the nanoparticle surface often hinders the formation of multidentate ligands, which are crucial for creating efficient catalytic sites. This limitation, coupled with the complex and costly synthesis of pre-functionalized ligands, underscores the need for alternative support materials.

To address this challenge, acetylacetone (acac), a versatile β-diketone, emerges as a promising candidate. Acac can function as a bidentate ligand, forming stable complexes with metal ions.[37] Its two carbonyl groups provide opportunities for further functionalization through reactions with amines to generate Schiff base ligands.[38] The proximity of these carbonyl groups within the acac structure facilitates the formation of multidentate chelating systems.[39] Additionally, the active methylene group in acac allows for alkylation reactions,[40–42] enabling covalent attachment to various support and linker materials.

In this study, we aim to immobilize acetylacetone onto magnetic nanoparticles and subsequently synthesize a novel tetradentate salen-type Schiff base ligand and related complex through condensation with 2-picolylamine in the presence of $CuCl_2$. The resulting copper complex will be evaluated as a catalyst for 5-Substituted 1*H*-tetrazoles synthesis under green conditions.

2. Experimental

2.1. Typical procedure for synthesis of [Fe_3O_4@Sil-Schiff-base-Cu(II)] complex

The synthesis began with the preparation of Fe_3O_4 MNPs using a previously established method.[43] Concurrently, 2 g of Fe_3O_4 MNPs were dispersed in 100 milliliters of toluene for 30 minutes. Subsequently, 3-(3-trimethoxysilylpropyl)–acetylacetone (5 mmol) was introduced into the reaction mixture, which was then refluxed under vigorous stirring and a nitrogen (N_2) atmosphere for 12 hours. Following this, the resulting Fe_3O_4@Sil–acac MNPs product was magnetically isolated, washed ethanol (3 × 25 mL), and subsequently dried at 80 °C for 6 hours. Subsequently, 3 grams of Fe_3O_4@Sil–acac were dispersed in 100 mL of degassed ethanol through sonication for 30 minutes. Then, 2-picolylamine (10 mmol) and copper(II) nitrate trihydrate (5 mmol) were sequentially added to the prepared suspension, followed by refluxing under vigorous stirring and a N_2 atmosphere for 48 hours. Upon completion of the reaction, the [Fe_3O_4@Sil-Schiff-base-Cu(II)] complex was magnetically separated, washed multiple times with hot water and ethanol, and finally dried at 80 °C for 6 hours (Scheme 1).

2.2. General procedure for synthesis of 5-substituted 1*H*-tetrazoles catalyzed by [Fe_3O_4@Sil-Schiff-base-Cu(II)] complex

To a 2 mL solution of aryl nitrile (1 mmol) and sodium azide (1.3 mmol) in PEG-400, [Fe_3O_4@Sil-Schiff-base-Cu(II)] complex (5 mol%) was added. The mixture was stirred at 120 °C until reaction completion. After cooling to room temperature, the reaction mixture was diluted with hot water, and the catalyst was removed by magnetic separation. The aqueous phase was acidified to pH 1 with 1 M hydrochloric acid and extracted with ethyl acetate (45 mL). The organic phase was washed repeatedly with water, dried over magnesium sulfate, and concentrated under reduced pressure. The crude product was purified by preparative thin-layer chromatography (TLC).

3. Results and discussions

In this research, a novel Schiff base copper complex was synthesized *via* a three-step procedure. A template Hugo Schiff reaction of nanomagnetized acetyl acetone backbone with two equivalents of 2-picolylamine in the presence of one equivalent of copper salt, acting as both catalyst and coordination partner, yielded the desired five-coordinate copper(II) complex as the stabilized catalytic site (Scheme 1). The structure of the prepared nanoparticles was comprehensively characterized

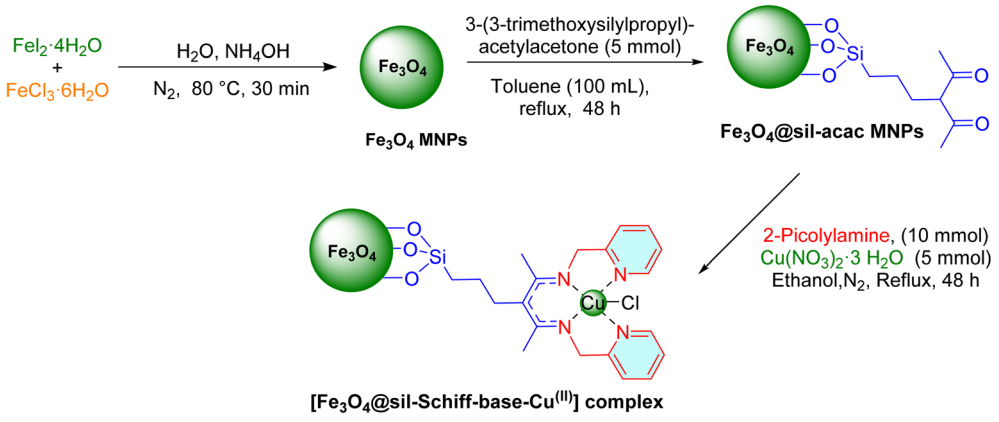

Scheme 1 Stepwise synthesis of [Fe_3O_4@Sil-Schiff-base-Cu(II)] complex.

using FT-IR, XRD, TGA, EDAX, ICP-OES, EDS mapping, FE-SEM, TEM, and VSM analyses.

3.1. Catalyst characterization

Fig. 1 presents the FT-IR spectra of Fe_3O_4, Fe_3O_4@Sil–acac, and the [Fe_3O_4@Sil-Schiff-base-Cu(II)] complex. Broad absorption band centered at around 3400 cm^{-1} is observed in the curve *a*, indicative of hydroxyl groups, likely attributable to adsorbed water or surface hydroxyl functionalities. The characteristic peaks at 568 and 634 cm^{-1} correspond to Fe–O vibrations within the iron oxide lattice, confirming the formation of the Fe_3O_4 MNPs.[44] The spectrum of Fe_3O_4@Sil-acac exhibits additional bands at around 2900 cm^{-1}, 1715 cm^{-1}, and 1063 cm^{-1}. These features can be assigned to C–H stretching, C=O stretching, and Si–O–Si stretching vibrations, respectively. The emergence of the Si–O–Si band confirms the successful immobilization of Sil–acac onto the Fe_3O_4 nanoparticles. In the spectrum of the [Fe_3O_4@Sil-c-Cu(II)] complex, the disappearance of the C=O band and the concomitant appearance of new peaks around 1637 cm^{-1} strongly suggest the formation of the Schiff base and subsequent complexation with Cu(II) ions. These spectral alterations collectively provide evidence for the successful introduction of organic functionalities onto the Fe_3O_4 surface and the formation of the desired complex.

Structural characterization of the [Fe_3O_4@Schiff-base-Cu(II)] complex was performed using X-ray diffraction (XRD) in the 10–80° 2θ range (Fig. 2). Characteristic peaks corresponding to magnetite (Fe_3O_4) were observed at 2θ values of 30.02°, 35.31°, 43.22°, 53.19°, 56.89°, and 62.89° which are corresponded to (220), (311), (222), (400), (422), (511), (440), lattice planes of Fe_3O_4 and confirming the successful incorporation of magnetic nanoparticles. Additional peaks at 2θ values of 32.67°, 36.21°, 39.43°, 49°, 54°, and 60.29° suggest the presence of copper and the formation of a Schiff base–Cu complex on the Fe_3O_4 surface.

Thermogravimetric analysis (TGA) was conducted to assess the thermal stability of pristine Fe_3O_4 nanoparticles in comparison to their corresponding [Fe_3O_4@Sil-Schiff-base-Cu(II)] complex (Fig. 3). The pristine Fe_3O_4 nanoparticles exhibited negligible weight loss across the entire temperature range, indicative of their high thermal stability. In contrast, the [Fe_3O_4@Schiff-base-Cu(II)] complex demonstrated a pronounced two-step weight loss profile. The weight loss occurring between 200 and 600 °C is attributed to the decomposition of the organic silane linker and Schiff base ligand situated on the Fe_3O_4 surface. These findings collectively highlight the substantial influence of the organic coating on the thermal properties of the composite material and corroborate the successful formation of the [Schiff-base-Cu(II)] complex on the Fe_3O_4 surface.

EDAX analysis confirms the successful synthesis of the [Fe_3O_4@Sil-Schiff-base-Cu(II)] complex. The detected elements, including Fe, O, Si, C, N, Cu, and Cl, are consistent with the theoretical composition of the material (Fig. 4). The sharp peaks associated with Fe and O suggest the presence of Fe_3O_4 nanoparticles, while the detection of Si confirms the integration of the organosilica linker. The presence of C and N is indicative of

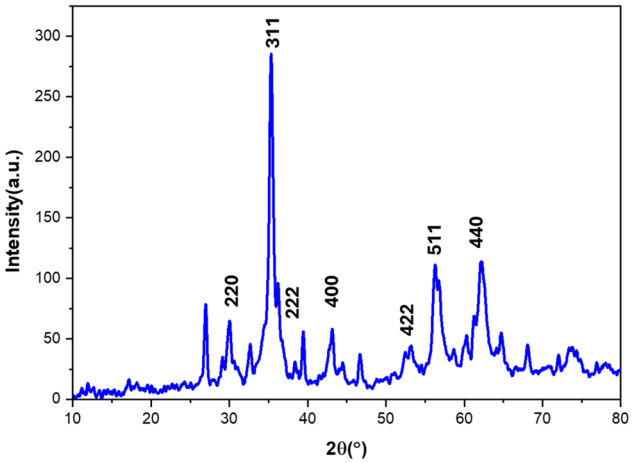

Fig. 2 XRD analysis of [Fe_3O_4@Sil-Schiff-base-Cu(II)] complex.

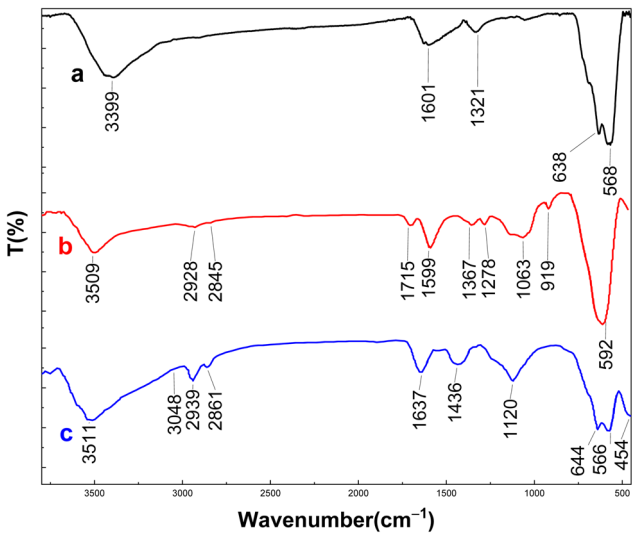

Fig. 1 FT-IR analysis of (a) Fe_3O_4, (b) Fe_3O_4@Sil–acac and (c) [Fe_3O_4@Sil-Schiff-base-Cu(II)] complex.

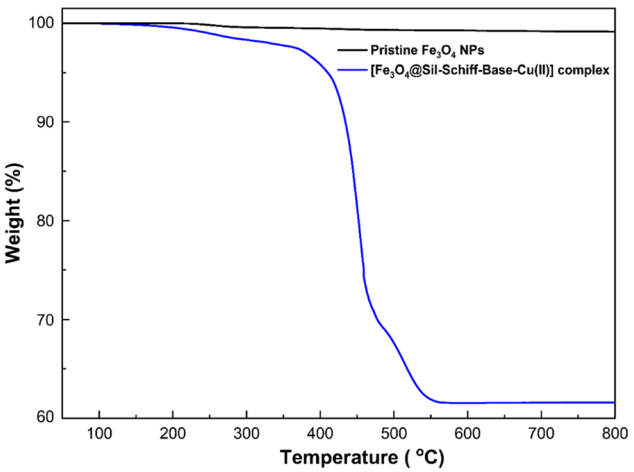

Fig. 3 TGA curves of pristine Fe_3O_4 NPs and [Fe_3O_4@Sil-Schiff-base-Cu(II)] complex.

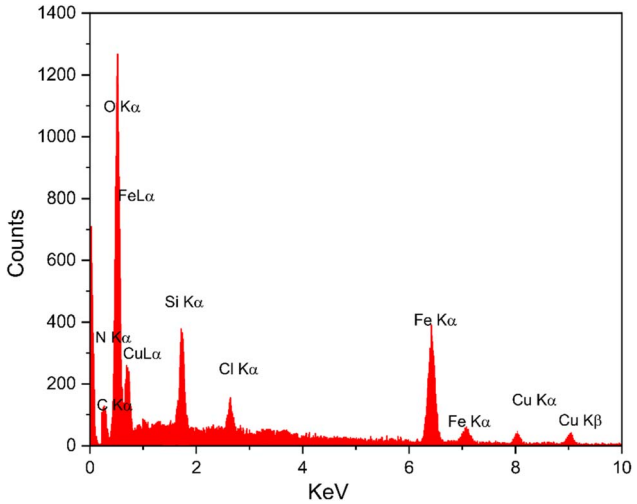

Fig. 4 EDAX analysis of [Fe_3O_4@Sil-Schiff-base-Cu(II)] complex.

the Schiff base ligand, and the detection of Cu verifies the coordination of the copper ion to the ligand. The identified chlorine supports its role in the formation of a five-coordinate copper(II) complex *via* coordination to the copper precursor. Additionally, ICP-OES analysis revealed a copper content of approximately 1.73×10^{-3} mol g^{-1} in the sample.

EDAX mapping indicates a widespread distribution of Fe and O, suggesting the formation of Fe_3O_4. The mapping also revealed a homogeneous distribution of Si, C, and N elements throughout the Fe_3O_4 support, implying the presence of nitrogen-containing functional groups (Fig. 5). However, the silicon content appears lower than that of carbon and nitrogen, aligning with its approximate proportion in the stabilized complex composition. Conversely, copper and chlorine elements show a uniform distribution across the surface, facilitating optimal accessibility for guest reactant species.

SEM analysis of the [Fe_3O_4@Sil-Schiff-base-Cu(II)] complex revealed a heterogeneous population of agglomerated spherical particles with rough surface textures (Fig. 6). The particles exhibited a broad size distribution, averaging approximately 47.46 nm in diameter. These morphological features suggest a complex microstructure composed of both agglomerated and discrete nanoparticles.

TEM analysis of [Fe_3O_4@Sil-Schiff-base-Cu(II)] complexes revealed well-defined, spherical nanoparticles with a smooth surface and a narrow size distribution centered around 20–25 nm (Fig. 7). These nanoparticles were evenly dispersed without aggregation, indicating high-quality synthesis. These characteristics, including uniform shape and size, suggest promising potential for various applications due to the nanoparticles' consistent behavior and reactivity.

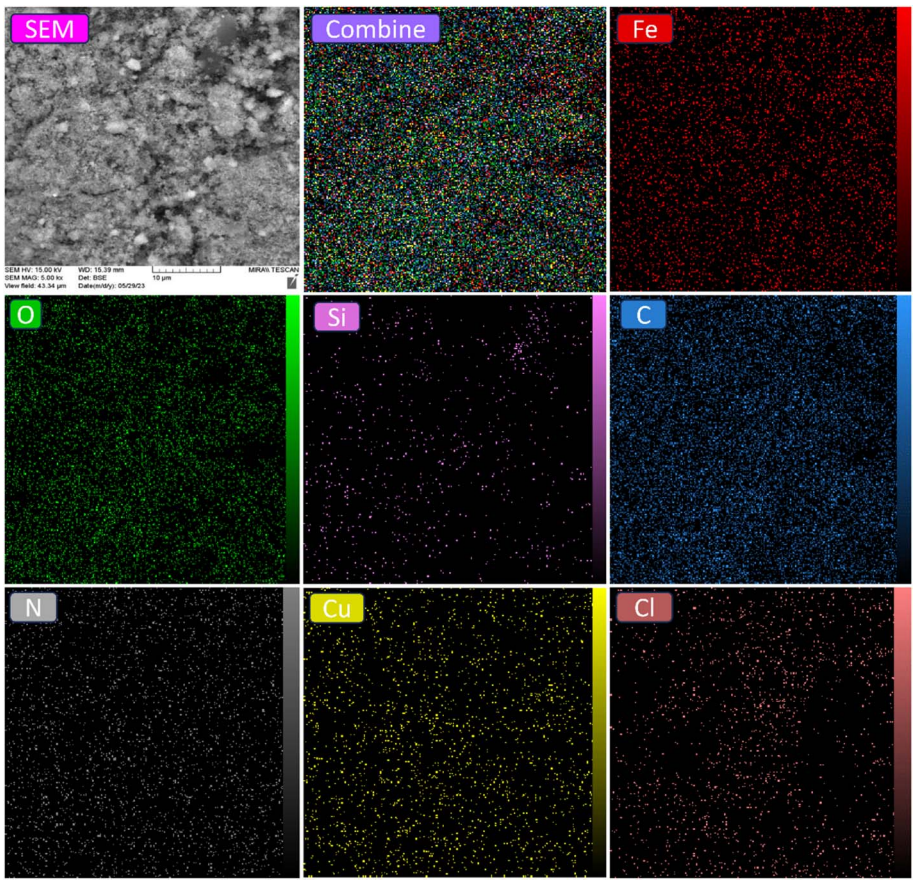

Fig. 5 Elemental mapping images of [Fe_3O_4@Sil-Schiff-base-Cu(II)] complex.

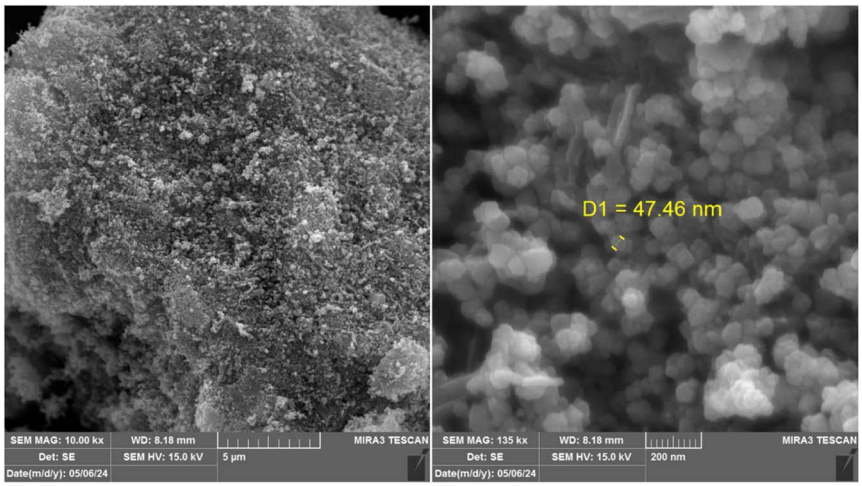

Fig. 6 SEM images of [Fe_3O_4@Sil-Schiff-base-Cu(II)] complex.

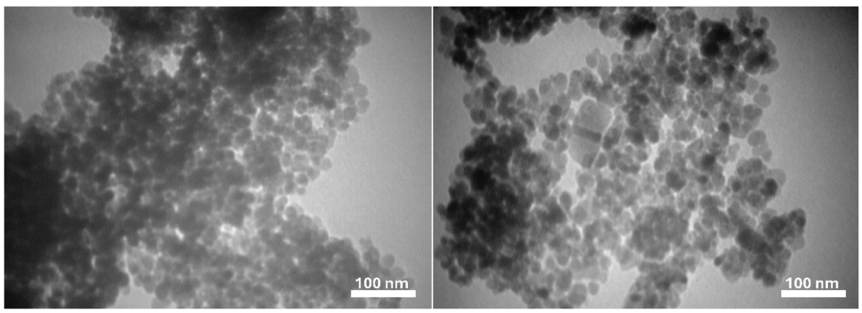

Fig. 7 TEM images of [Fe_3O_4@Sil-Schiff-base-Cu(II)] complex.

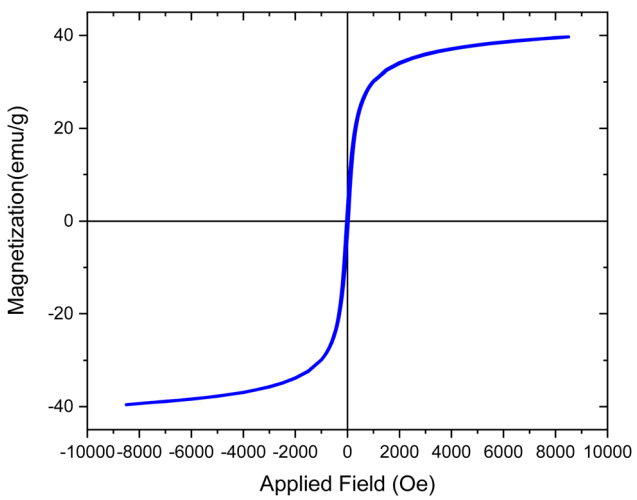

Fig. 8 VSM analysis of [Fe_3O_4@Sil-Schiff-base-Cu(II)] complex.

VSM analysis corroborated ferromagnetic behavior for the [Fe_3O_4@Sil-Schiff-base-Cu(II)] complex, as evidenced by a hysteresis loop (Fig. 8). This finding indicates the retention of Fe_3O_4 intrinsic magnetic properties. Nevertheless, the complex exhibited a reduced saturation magnetization (Ms = 39.87 emu g^{-1}) compared to pristine Fe_3O_4 (Ms ≈ 63 emu g^{-1}),[45] indicating a lower magnetic moment. Conversely, an augmented coercivity was observed, implying enhanced resistance to magnetic field reversal. These magnetic property modifications are likely attributable to surface interactions, potential spin canting, and magnetic dilution arising from the organic ligand, which confirm the successful stabilization of [Sil-Schiff-base-Cu(II)] complex on Fe_3O_4 surface.

The [Fe_3O_4@Sil-Schiff-base-Cu(II)] complex exhibits a moderate BET surface area of 145.17 m^2 g^{-1}, indicating a sufficient surface area for adsorption (Fig. 9). The total pore volume of 0.1375 cm^3 g^{-1} and mean pore diameter of 17.369 nm reveal a relatively narrow pore size distribution. t-plot and BJH analyses further confirm the micropore volume and pore size distribution characteristics of the catalyst. These combined properties make the catalyst well-suited for a range of applications in heterogeneous catalysis processes.

3.2. Catalytic study

The catalytic efficacy of the [Fe_3O_4@Sil-Schiff-base-Cu(II)] complex was evaluated in the click reaction of benzonitrile and sodium azide for the synthesis of 5-substituted 1*H*-tetrazoles, serving as a model reaction for the optimization of effective reaction parameters (Table 1). Blank test demonstrated that the reaction did not proceed in the absence of a catalyst, even after

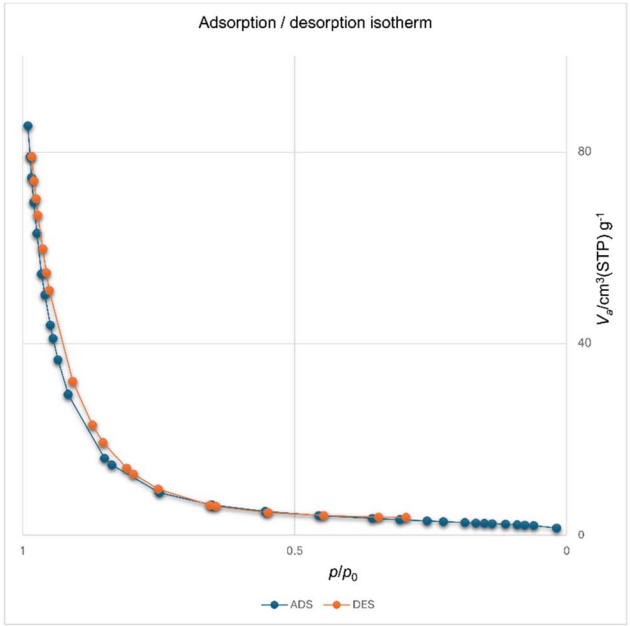

Fig. 9 N_2 adsorption/desorption isotherms of [Fe_3O_4@Sil-Schiff-base-Cu(II)] complex.

a long reaction time of 10 hours (Table 1, entry 1). Upon introduction of the [Fe_3O_4@Sil-Schiff-base-Cu(II)] complex to the reaction mixture, the conversion initiated, with a concomitant increase in yield as the catalyst loading was augmented. Optimal results were achieved with a 5 mg catalyst loading, affording complete conversion within 10 minutes. Further increasing of the catalyst amount to 7 mg did not result in enhanced reaction kinetics or product yield. Given the established utility of polyethylene glycols as solvents in analogous processes, the influence of average molecular weight on the current reaction was examined. While comparable results were obtained across different polyethylene glycol variants, PEG-400 exhibited marginally superior performance and was consequently selected as the optimal solvent. A reduction in reaction temperature led to diminished product yields, thereby establishing 120 °C as the preferred reaction temperature.

The optimized method was applied to a diverse array of aryl nitriles to assess the method scope and the influence of electronic and steric factors on reaction efficiency (Table 2). Electron-withdrawing substituents on aryl nitriles exhibited enhanced reactivity compared to electron-donating groups due to increased electrophilicity of the nitrile carbon. Furthermore, the substituent's position significantly impacted reactivity, with *ortho* substituents generally affording lower yields and requiring longer reaction times than their para counterparts. This behavior can be attributed to both steric hindrance and electronic effects. Despite these variations, the majority of investigated aryl nitriles produced the corresponding products in satisfactory to excellent yields. To assess the selectivity of our method, we conducted comparative experiments with aliphatic nitriles. Under identical reaction conditions, no product formation was observed after 4 hours, suggesting a high degree of selectivity toward aromatic nitriles. This selectivity allows for the selective conversion of aromatic nitriles to tetrazole derivatives in the presence of aliphatic nitrile functionalities without interference.

The proposed mechanism for the synthesis of 5-aryl-1*H*-tetrazoles catalyzed by [Fe_3O_4@Sil-Schiff-base-Cu(II)] is outlined in Scheme 2.[6,57,58] The catalytic cycle is initiated by the

Table 1 Optimization of click reaction of benzonitrile and sodium azide over the catalysis of [Fe_3O_4@Sil-Schiff-base-Cu(II)] complex

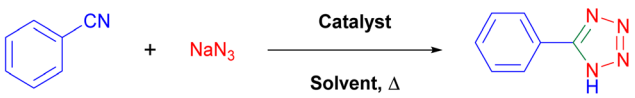

Entry	Amount of catalyst (mol%)	Solvent	Temperature (°C)	Time (min)	Yield[a,b] (%)
1	—	PEG-400	120	600	NR
2	1	PEG-400	120	10	64
3	2	PEG-400	120	10	72
4	4	PEG-400	120	10	93
5	5	PEG-400	120	10	99
6	7	PEG-400	120	10	99
7	5	Ethanol	120	10	43
8	5	Ethylene glycol	120	10	71
9	5	PEG-200	120	10	98
10	5	PEG-600	120	10	98
11	5	PEG-1000	120	10	95
12	5	PEG-400	90	10	88
13	5	PEG-400	60	10	53
14	5	PEG-400	40	10	24
15	5	PEG-400	r. t.	10	NR

[a] Isolated yield. [b] Conditions: benzonitrile (1 mmol), sodium azide (1.3 mmol), [Fe_3O_4@Sil-Schiff-base-Cu(II)] complex (mol%) and solvent (2 mL).

Table 2 The scope of click condensation of aryl nitriles and sodium azide over the catalysis of [Fe_3O_4@Sil-Schiff-base-Cu(II)] complex

Entry	Aryl nitrile	Product	Time (min)	Yield[a,b] (%)	TON	TOF (min^{-1})	M. P.	Ref.
1	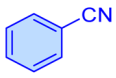	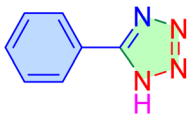	10	98	1960	10 172	219–221	46
2	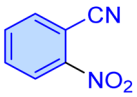	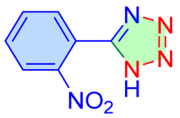	25	91	10 520	25 248	158–161	47
3	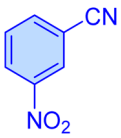	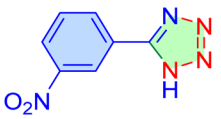	12	97	11 213	56 069	155–157	46
4	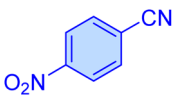	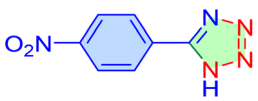	10	99	11 445	68 670	220–22	46
5	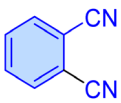	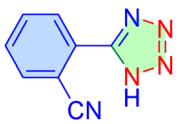	25	89	10 289	24 693	209–211	48
6	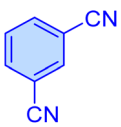	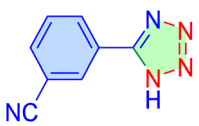	15	96	11 098	44 393	210–212	48
7	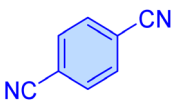	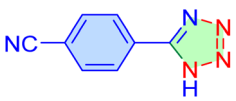	8	98	11 329	84 971	254–256	48
8	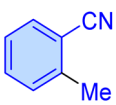	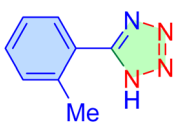	20	88	10 173	30 520	153–155	49
9	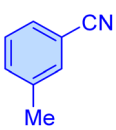	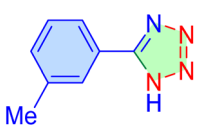	15	95	10 982	43 930	151–152	50
10	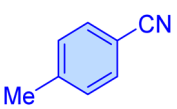	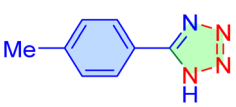	15	95	10 982	43 930	248–25	46
11	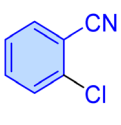	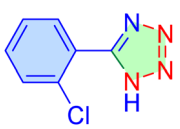	20	93	10 751	32 254	180–181	51
12	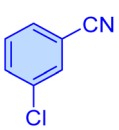	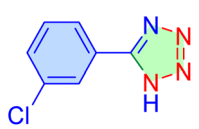	15	97	11 213	44 855	139–141	52
13	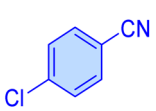	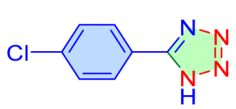	10	98	11 329	67 976	155–156	46

Table 2 (*Contd.*)

Entry	Aryl nitrile	Product	Time (min)	Yield[a,b] (%)	TON	TOF (min^{-1})	M. P.	Ref.
14	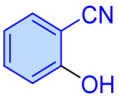	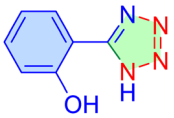	45	89	10 289	13 718	224–225	53
15	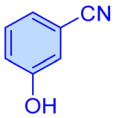	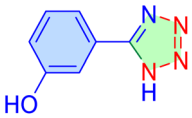	20	95	10 982	32 947	245–246	54
16	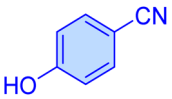	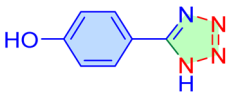	30	93	10 751	21 502	233–23	46
17	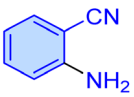	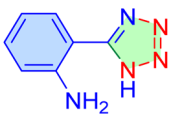	65	86	9942	9177	220–222	55
18		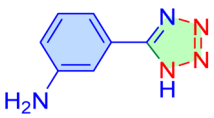	20	95	10 982	32 946	199–200	56
19	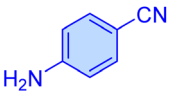	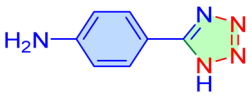	40	91	10 520	15 780	266–268	46
20		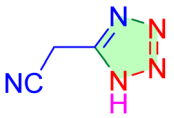	240	N. R.	—	—	—	—
21		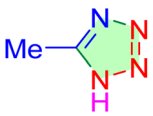	240	N. R.	—	—	—	—

[a] Isolated yield. [b] Conditions: aryl nitrile (1.0 mmol), sodium azide (1.3 mmol) and [Fe_3O_4@Sil-Schiff-base-Cu(II)] complex (5 mg) in PEG-400 (1 mL) at 120 °C.

coordination of the nitrile substrate to the copper center within the catalyst, thereby activating the nitrile group. Subsequently, a nucleophilic attack of the azide ion on the activated nitrile species triggers a [2 + 3] cycloaddition cascade, resulting in the formation of the tetrazole ring. The reaction is finalized during the workup stage, where acidification protonates the intermediate sodium salt to afford the desired 5-aryl-1*H*-tetrazole product.

3.3. Reusability of catalyst

To evaluate the [Fe_3O_4@Sil-Schiff-base-Cu(II)] complex recyclability, it was magnetically separated from the reaction mixture after each cycle using an external magnet, followed by washing with hot ethanol and water. The recovered catalyst was reused in subsequent reaction cycles without significant loss of activity, demonstrating its robustness and potential for multiple applications. The catalyst exhibited consistent catalytic performance over eight consecutive cycles, highlighting its promising recyclability and economic viability (Fig. 10). To assess the structural integrity and functional group composition of the recovered catalyst, FT-IR analysis was conducted. As depicted in Fig. 11, the spectrum closely resembles that of the pristine catalyst, indicating its structural stability.

3.4. Hot filtration test

To investigate the heterogeneous nature of the [Fe_3O_4@Sil-Schiff-base-Cu(II)] catalyst, a hot filtration test was performed. At the midpoint of the reaction, the catalyst was magnetically separated from the reaction mixture, which was subsequently allowed to proceed for an additional eight hours. The negligible

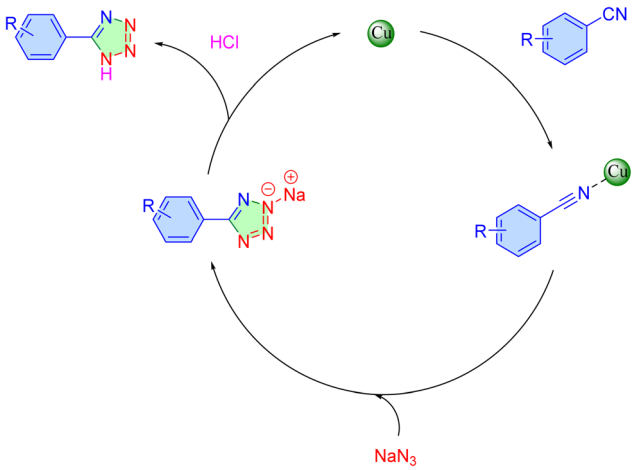

Scheme 2 Possible mechanism for the click condensation of aryl nitriles and sodium azide over the catalysis of [Fe_3O_4@Sil-Schiff-base-Cu(II)] complex.

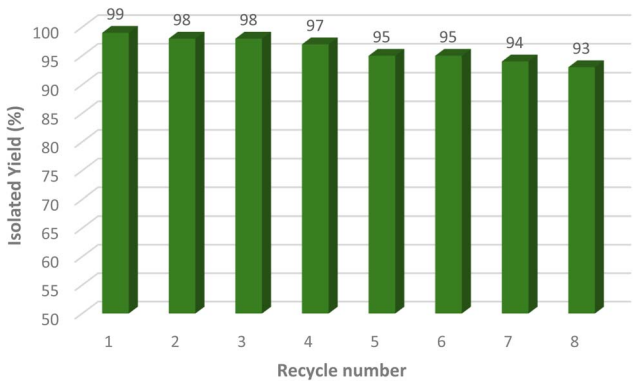

Fig. 10 The reusability of [Fe_3O_4@Sil-Schiff-base-Cu(II)] complex.

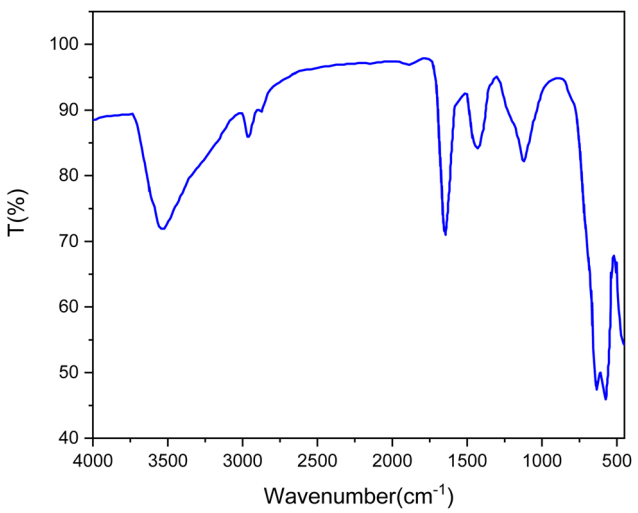

Fig. 11 FT-IR analysis of recovered [Fe_3O_4@Sil-Schiff-base-Cu(II)] catalyst.

product formation observed post-filtration confirmed the catalyst's predominantly heterogeneous character and indicated minimal metal leaching.

Table 3 Comparison the efficiency of [Fe_3O_4@Sil-Schiff-base-Cu(II)] complex click reaction

Entry	Catalyst	Time (min)	Yield (%)	Reference
1	$CoFe_2O_4$/MCM-41/PA/Cu	20	91	59
2	Amberlyst-15	720	91	60
3	$ZnFe_2O_4$@SiO_2–SO_3H	60	100	61
4	$CuFe_2O_4$@SiO_2–MnCl	60	97.8	62
5	Cu–Amd–RGO	30	96	63
6	CAES	60	95	64
7	f Cu–DPMI@biochar	60	98	65
8	MCM-41@Gln@Cu–Fe	25	73	66
9	[Fe_3O_4@Sil-schiff-base-Cu(II)]	10	99	This work

3.5. Comparison study of catalytic activity

A comparative analysis of the catalytic efficiency of the herein reported [Fe_3O_4@Sil-Schiff-base-Cu(II)] catalyst with those previously documented in the literature was conducted, with particular attention to reaction conditions and isolated product yields (Table 3). While prior studies exhibit commendable attributes, they often necessitate extended reaction times, high catalyst loadings, or the employment of precious metal catalysts. In contrast, the Cu complexes presented herein demonstrate competitive product yields, coupled with advantages such as reduced catalyst loading, enhanced turnover frequencies, facile separation protocols, the use of environmentally conditions, and the absence of hazardous byproducts.

Conclusions

A novel copper(II) bis-Schiff base complex was synthesized through post-synthetic modification of nanomagnetic Fe_3O_4 using HNacNac and pyridine building blocks. The complex features a tetradentate N_4 coordination sphere, resulting in a five-coordinate copper center upon reaction with $CuCl_2$. The resulting complex exhibited high catalytic activity in the synthesis of 5-substituted 1*H*-tetrazoles from diverse aromatic nitriles and sodium azide under mild conditions. The catalyst performance was influenced by electronic and steric factors of the substrates. Remarkably, the catalyst demonstrated exceptional stability and reusability, maintaining its catalytic activity over eight consecutive cycles without significant loss of efficiency. This work introduces a promising and sustainable catalytic system for the efficient production of tetrazoles.

Data availability

The authors declare that all the data in this manuscript are available upon request.

Author contributions

Chou-Yi Hsu: characterization of catalyst. Ahmed Rafiq AlBajalan: conceptualization, analysis, review draft, acquiring research funding and supervision. Sameer A. Awad: writing original draft, laboratory works. Muath Suliman: laboratory

works. Nizomiddin Juraev: catalysis studies and analysis. Carlos Rodriguez-Benites: software and review/editing. Hamad AlMohamadi: conceptualization, laboratory works, analysis, review/editing. Abed J. Kadhim: software and review/editing.

Conflicts of interest

The authors declare that they have no competing interests.

Acknowledgements

The authors express their gratitude to the Deanship of Scientific Research at King Khalid University for funding this work through the Large Research Group Project under grant number RGP.02/375/44.

References

1 C. G. Neochoritis, T. Zhao and A. Dömling, Tetrazoles via Multicomponent Reactions, *Chem. Rev.*, 2019, **119**, 1970–2042.
2 N. Dhiman, K. Kaur and V. Jaitak, Tetrazoles as anticancer agents: A review on synthetic strategies, mechanism of action and SAR studies, *Bioorg. Med. Chem.*, 2020, **28**, 115599.
3 A. Maleki and A. Sarvary, Synthesis of tetrazoles via isocyanide-based reactions, *RSC Adv.*, 2015, **5**, 60938–60955.
4 M. M. Maseer, T. Kikhavani and B. Tahmasbi, A multidentate copper complex on magnetic biochar nanoparticles as a practical and recoverable nanocatalyst for the selective synthesis of tetrazole derivatives, *Nanoscale Adv.*, 2024, **6**, 3948–3960.
5 G. Baskaya, İ. Esirden, E. Erken, *et al.*, Synthesis of 5-Substituted-1H-Tetrazole Derivatives Using Monodisperse Carbon Black Decorated Pt Nanoparticles as Heterogeneous Nanocatalysts, *J. Nanosci. Nanotechnol.*, 2017, **17**, 1992–1999.
6 S. M. Joshi, R. B. Mane, K. R. Pulagam, *et al.*, The microwave-assisted synthesis of 5-substituted 1: H -tetrazoles via [3+2] cycloaddition over a heterogeneous Cu-based catalyst: Application to the preparation of 13N-labelled tetrazoles, *New J. Chem.*, 2017, **41**, 8084–8091.
7 H. C. Du, M. M. Matzuk and Y. C. Chen, Synthesis of 5-substituted tetrazoles: via DNA-conjugated nitrile, *Org. Biomol. Chem.*, 2020, **18**, 9221–9226.
8 S. Swami, S. N. Sahu and R. Shrivastava, Nanomaterial catalyzed green synthesis of tetrazoles and its derivatives: a review on recent advancements, *RSC Adv.*, 2021, **11**, 39058–39086.
9 M. Aldhoun, A. Massi and A. Dondoni, Click Azide−Nitrile Cycloaddition as a New Ligation Tool for the Synthesis of Tetrazole-Tethered C -Glycosyl α-Amino Acids, *J. Org. Chem.*, 2008, **73**, 9565–9575.
10 L. V. Myznikov, U. N. Dmitrieva, T. V. Artamonova, *et al.*, Tetrazoles: LVII. Preparation and chemical properties of 1-substituted 5-arylsulfonyltetrazoles, *Russ. J. Org. Chem.*, 2013, **49**, 754–757.
11 S. Krištafor, A. Bistrović, J. Plavec, *et al.*, One-pot click synthesis of 1,2,3-triazole-embedded unsaturated uracil derivatives and hybrids of 1,5- and 2,5-disubstituted tetrazoles and pyrimidines, *Tetrahedron Lett.*, 2015, **56**, 1222–1228.
12 S. M. Kondengadan, S. Bansal, C. Yang, *et al.*, Click chemistry and drug delivery: A bird's-eye view, *Acta Pharm. Sin. B*, 2023, **13**, 1990–2016.
13 M. Mohammadi, M. Khodamorady, B. Tahmasbi, *et al.*, Boehmite nanoparticles as versatile support for organic–inorganic hybrid materials: Synthesis, functionalization, and applications in eco-friendly catalysis, *J. Ind. Eng. Chem.*, 2021, **97**, 1–78.
14 R. Bikas, N. Heydari and T. Lis, Catalytic synthesis of tetrazoles by a silica supported Zn(II) coordination compound containing azide ligand, *J. Mol. Struct.*, 2023, **1281**, 135120.
15 S. V. Voitekhovich, O. A. Ivashkevich and P. N. Gaponik, Synthesis, properties, and structure of tetrazoles: Certain achievements and prospects, *Russ. J. Org. Chem.*, 2013, **49**, 635–654.
16 M. C. Bryan, P. J. Dunn, D. Entwistle, *et al.*, Key Green Chemistry research areas from a pharmaceutical manufacturers' perspective revisited, *Green Chem.*, 2018, **20**, 5082–5103.
17 S. G. Koenig, D. K. Leahy and A. S. Wells, Evaluating the Impact of a Decade of Funding from the Green Chemistry Institute Pharmaceutical Roundtable, *Org. Process Res. Dev.*, 2018, **22**, 1344–1359.
18 M. Kazemi, Copper Catalysts Immobilized on Magnetic Nanoparticles: Catalysis in Synthesis of Tetrazoles, *Nanomater. Chem.*, 2023, **1**, 1–11.
19 S. Leyva-Ramos, Recent Developments in the Synthesis of Tetrazoles and their Pharmacological Relevance, *Curr. Org. Chem.*, 2022, **25**, 388–403.
20 E. A. Popova, A. V. Protas and R. E. Trifonov, Tetrazole Derivatives as Promising Anticancer Agents, *Anti-Cancer Agents Med. Chem.*, 2018, **17**, 1856–1868.
21 B. Chen, H. Lu, J. Chen, *et al.*, Recent Progress on Nitrogen-Rich Energetic Materials Based on Tetrazole Skeleton, *Top. Curr. Chem.*, 2023, **381**, 25.
22 A. Singh and A. Agarwal, Anchoring CuO nanoparticle on nitrogen-doped reduced graphene oxide as nanocatalyst for the synthesis of 5-substituted-1H-tetrazole and 1,2,3-triazole derivatives, *Mol. Catal.*, 2023, **547**, 113377.
23 M. Ghadermazi, S. Molaei and S. Khorami, Synthesis, characterization and catalytic activity of copper deposited on MCM-41 in the synthesis of 5-substituted 1H-tetrazoles, *J. Porous Mater.*, 2023, **30**, 949–963.
24 A. Singh and A. Agarwal, Anchoring CuO nanoparticle on nitrogen-doped reduced graphene oxide as nanocatalyst for the synthesis of 5-substituted-1H-tetrazole and 1,2,3-triazole derivatives, *Mol. Catal.*, 2023, **547**, 113377.
25 A. Alexis Ramírez-Coronel, R. Sivaraman, Y. M. Ahmed, *et al.*, A Green and Ecofriendly Catalytic System for One-Pot Three-Component Synthesis of 5-Substituted 1H-Tetrazoles Under

Microwave Irradiation, *Polycyclic Aromat. Compd.*, 2024, **44**, 577–590.
26 Y. S. Priyanka, P. Rana, *et al.*, Unexplored catalytic potency of a magnetic CoFe2O4/Ni-BDC MOF composite for the one-pot sustainable synthesis of 5-substituted 1-H tetrazoles, *Chem. Eng. J.*, 2024, **496**, 153995.
27 S. Khizar, N. M. Ahmad, N. Zine, *et al.*, Magnetic Nanoparticles: From Synthesis to Theranostic Applications, *ACS Appl. Nano Mater.*, 2021, **4**, 4284–4306.
28 Z. Ma, J. Mohapatra, K. Wei, *et al.*, Magnetic Nanoparticles: Synthesis, Anisotropy, and Applications, *Chem. Rev.*, 2023, **123**, 3904–3943.
29 Q. Zhang, X. Yang and J. Guan, Applications of Magnetic Nanomaterials in Heterogeneous Catalysis, *ACS Appl. Nano Mater.*, 2019, **2**, 4681–4697.
30 M. Nasrollahzadeh, Advances in Magnetic Nanoparticles-Supported Palladium Complexes for Coupling Reactions, *Molecules*, 2018, **23**, 2532.
31 R. Dalpozzo, Magnetic nanoparticle supports for asymmetric catalysts, *Green Chem.*, 2015, **17**, 3671–3686.
32 J. Rakhtshah, A comprehensive review on the synthesis, characterization, and catalytic application of transition-metal Schiff-base complexes immobilized on magnetic Fe3O4 nanoparticles, *Coord. Chem. Rev.*, 2022, **467**, 214614.
33 C. Boulechfar, H. Ferkous, A. Delimi, *et al.*, Schiff bases and their metal Complexes: A review on the history, synthesis, and applications, *Inorg. Chem. Commun.*, 2023, **150**, 110451.
34 J. Rakhtshah, A comprehensive review on the synthesis, characterization, and catalytic application of transition-metal Schiff-base complexes immobilized on magnetic Fe3O4 nanoparticles, *Coord. Chem. Rev.*, 2022, **467**, 214614.
35 A. Ghorbani-Choghamarani, Z. Darvishnejad and M. Norouzi, Synthesis and characterization of copper(II) Schiff base complex supported on Fe 3 O 4 magnetic nanoparticles: a recyclable catalyst for the one-pot synthesis of 2,3-dihydroquinazolin-4(1H)-ones, *Appl. Organomet. Chem.*, 2015, **29**, 707–711.
36 M. Pawlaczyk, R. Frański, M. Cegłowski, *et al.*, Mass Spectrometric Investigation of Organo-Functionalized Magnetic Nanoparticles Binding Properties toward Chalcones, *Materials*, 2021, **14**, 4705.
37 M. Kremer and U. Englert, N Donor substituted acetylacetones – versatile ditopic ligands, *Z. Kristallogr.–Cryst. Mater.*, 2018, **233**, 437–452.
38 S. K. Gupta, P. B. Hitchcock and Y. S. Kushwah, Synthesis, Characterization and Crystal Structure of a Nickel(II) Schiff Base Complex Derived from Acetylacetone and Ethylenediamine, *J. Coord. Chem.*, 2002, **55**, 1401–1407.
39 G. O. Dudek and R. H. Holm, A Proton Resonance Study of Bis-(acetylacetone)-ethylenediimine and Related Schiff Bases, *J. Am. Chem. Soc.*, 1961, **83**, 2099–2104.
40 B. Bisek and W. Chaładaj, Access to 2-Alkenyl-furans via a Cascade of Pd-Catalyzed Cyclization/Coupling Followed by Oxidative Aromatization with DDQ, *J. Org. Chem.*, 2024, **89**, 7275–7279.
41 A. Shrinidhi and C. L. Perrin, Nucleophilic Addition of Enolates to 1,4-Dehydrobenzene Diradicals Derived from Enediynes: Synthesis of Functionalized Aromatics, *ACS Omega*, 2022, **7**, 22930–22937.
42 F.-X. Wang, J.-L. Yan, Z. Liu, *et al.*, Assembly of multicyclic isoquinoline scaffolds from pyridines: formal total synthesis of fredericamycin A, *Chem. Sci.*, 2021, **12**, 10259–10265.
43 Y. Wei, B. Han, X. Hu, *et al.*, Synthesis of Fe3O4 Nanoparticles and their Magnetic Properties, *Procedia Eng.*, 2012, **27**, 632–637.
44 A. E. Ferenj, D. M. Kabtamu, A. H. Assen, *et al.*, Hagenia abyssinica-Biomediated Synthesis of a Magnetic Fe3O4/NiO Nanoadsorbent for Adsorption of Lead from Wastewater, *ACS Omega*, 2024, **9**, 6803–6814.
45 F. Alemi-Tameh, J. Safaei-Ghomi, M. Mahmoudi-Hashemi, *et al.*, A comparative study on the catalytic activity of Fe3O4@SiO2–SO3H and Fe3O4@SiO2–NH2 nanoparticles for the synthesis of spiro [chromeno [2, 3-c] pyrazole-4, 3′-indoline]-diones under mild conditions, *Res. Chem. Intermed.*, 2016, **42**, 6391–6406.
46 Z. He, L. Feng, P. Wu, *et al.*, A Top-Down Approach to Synthesis of pH-Controlled Cu NPs: Their Catalytic Activity toward the One-Pot Preparation of α-Aminonitriles and 5-Substituted 1H-Tetrazoles from Aldehydes, *ChemistrySelect*, 2020, **5**, 7753–7767.
47 J. Bonnamour and C. Bolm, Iron salts in the catalyzed synthesis of 5-substituted 1H-tetrazoles, *Chem.–Eur. J.*, 2009, **15**, 4543–4545.
48 M. Esmaeilpour, J. Javidi and S. Zahmatkesh, One-pot synthesis of 1- and 5-substituted 1 H -tetrazoles using 1,4-dihydroxyanthraquinone–copper(II) supported on superparamagnetic Fe 3 O 4 @SiO 2 magnetic porous nanospheres as a recyclable catalyst, *Appl. Organomet. Chem.*, 2016, **30**, 897–904.
49 A. M. Liao, T. Wang, B. Cai, *et al.*, Design, synthesis and evaluation of 5-substituted 1-H-tetrazoles as potent anticonvulsant agents, *Arch. Pharmacal Res.*, 2017, **40**, 435–443.
50 Y. Zhu, Y. Ren and C. Cai, One-pot synthesis of 5-substituted lH-tetrazoles from aryl bromides with potassium hexakis(cyano-κC)ferrate(4 -)(K4[Fe(CN)6]) as cyanide source, *Helv. Chim. Acta*, 2009, **92**, 171–175.
51 S. Rostamizadeh, H. Ghaieni, R. Aryan, *et al.*, Zinc chloride catalyzed synthesis of 5-substituted 1H-tetrazoles under solvent free condition, *Chin. Chem. Lett.*, 2009, **20**, 1311–1314.
52 N. Nowrouzi, S. Farahi and M. Irajzadeh, 4-(N,N-Dimethylamino)pyridinium acetate as a recyclable catalyst for the synthesis of 5-substituted-1H-tetrazoles, *Tetrahedron Lett.*, 2015, **56**, 739–742.
53 M. Abdollahi-Alibeik and A. Moaddeli, Multi-component one-pot reaction of aldehyde, hydroxylamine and sodium azide catalyzed by Cu-MCM-41 nanoparticles: a novel method for the synthesis of 5-substituted 1H-tetrazole derivatives, *New J. Chem.*, 2015, **39**, 2116–2122.
54 P. Akbarzadeh, N. Koukabi and E. Kolvari, Anchoring of triethanolamine–Cu(II) complex on magnetic carbon nanotube as a promising recyclable catalyst for the

synthesis of 5-substituted 1H-tetrazoles from aldehydes, *Mol. Diversity*, 2020, **24**, 319–333.

55 S. A. Padvi and D. S. Dalal, Choline chloride–ZnCl 2 : Recyclable and efficient deep eutectic solvent for the [2+3] cycloaddition reaction of organic nitriles with sodium azide, *Synth. Commun.*, 2017, **47**, 779–787.

56 J. M. McManus and R. M. Herbst, Tetrazole Analogs of Aminobenzoic Acid Derivatives, *J. Org. Chem.*, 1959, **24**, 1044–1046.

57 R. S. B. Gonçalves and e M. L. S. de Mariz, Copper catalysis in the synthesis of 1,2,3-triazoles and tetrazoles, in *Copper in N-Heterocyclic Chemistry*, Elsevier, pp. , pp. 75–113.

58 M. Norouzi and S. Beiranvand, Fe3O4@SiO2@BHA-Cu(II) as a new, effective, and magnetically recoverable catalyst for the synthesis of polyhydroquinoline and tetrazole derivatives, *J. Chem. Sci.*, 2023, **135**, 86.

59 S. Molaei and M. Ghadermazi, Copper-decorated core–shell structured ordered mesoporous containing cobalt ferrite nanoparticles as high-performance heterogeneous catalyst toward synthesis of tetrazole, *Sci. Rep.*, 2023, **13**, 15146.

60 R. Shelkar, A. Singh and J. Nagarkar, Amberlyst-15 catalyzed synthesis of 5-substituted 1-H-tetrazole via [3+2] cycloaddition of nitriles and sodium azide, *Tetrahedron Lett.*, 2013, **54**, 106–109.

61 A. Nozari, H. Hassani and A. Karimian, ZnFe2O4@SiO2–SO3H Magnetic Nanoparticles: A New, Efficient, and Recyclable Heterogeneous Nanocatalyst for Successful Synthesis of 5-Substituted-1H-tetrazoles, *Russ. J. Org. Chem.*, 2023, **59**, 1370–1381.

62 M. Yousefizadeh, S. Saeednia, A. M. Hatefi, *et al.*, CuFe2O4@SiO2-LMnCl: an efficient, highly recyclable magnetic nanoparticle for synergic catalyzing of tetrazoles, *J. Iran. Chem. Soc.*, 2023, **20**, 1569–1578.

63 P. A. Kulkarni, A. K. Satpati, M. Thandavarayan, *et al.*, An efficient Cu/functionalized graphene oxide catalyst for synthesis of 5-substituted 1H-tetrazoles, *Chem. Pap.*, 2021, **75**, 2891–2899.

64 N. Razavi and B. Akhlaghinia, Cu(ii) immobilized on aminated epichlorohydrin activated silica (CAES): As a new, green and efficient nanocatalyst for preparation of 5-substituted-1H-tetrazoles, *RSC Adv.*, 2015, **5**, 12372–12381.

65 M. Alekasir, S. Heydarian and B. Tahmasbi, The synthesis of biochar from biomass waste recycling and its surface modification for immobilization of a new Cu complex as a reusable nanocatalyst in the homoselective synthesis of tetrazoles, *Res. Chem. Intermed.*, 2024, **50**, 2031–2049.

66 M. Ghadermazi, S. Molaei and S. M. Mousavipour, Nano Architectonics of Fe–Cu Bimetallic Particles Confined in a Mesoporous Silica Network for the Synthesis of 5-Substituted 1H-tetrazoles, *J. Inorg. Organomet. Polym. Mater.*, 2023, **33**, 3128–3145.